AD-A169 452 JOURNAL OF ENGINEERING THERMOPHYSICS (SELECTED ARTICLES)(U) FOREIGN TECHNOLOGY DIV WRIGHT-PATTERSON AFB OH D LIANFENG ET AL. 24 JUN 86 FTD-ID(RS)T-0312-86 1/1

UNCLASSIFIED F/G 13/7 NL

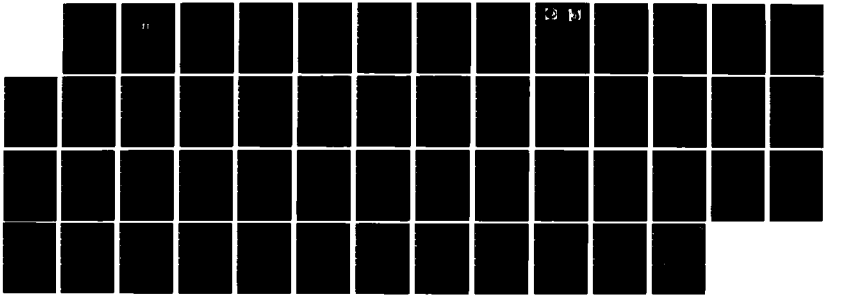

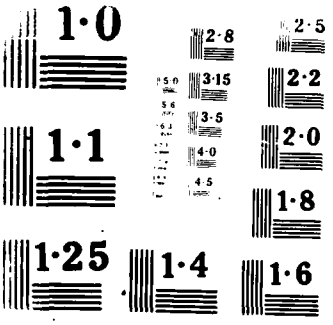
1·0
1·1
1·25
1·4
1·6
1·8
2·0
2·2
2·5
2·8
3·15
3·5
4·0
4·5

AD-A169 452

FTD-ID(RS)T-0312-86

FOREIGN TECHNOLOGY DIVISION

JOURNAL OF ENGINEERING THERMOPHYSICS

(Selected Articles)

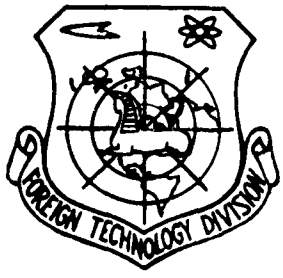

DTIC FILE COPY

Approved for public release;
Distribution unlimited.

86 7 7 036

HUMAN TRANSLATION

FTD-ID(RS)T-0312-86 24 June 1986

MICROFICHE NR: FTD-86-C-001960

JOURNAL OF ENGINEERING THERMOPHYSICS (Selected Articles)

English pages: 47

Source: Gongcheng Rewuli Xuebao, Vol. 3, Nr. 2, May 1982, pp. 123-130; 131-134; 135-137; 183-189.

Country of origin: China
Translated by: SCITRAN
F33657-84-D-0165
Requester: FTD/TQTA
Approved for public release; Distribution unlimited.

THIS TRANSLATION IS A RENDITION OF THE ORIGINAL FOREIGN TEXT WITHOUT ANY ANALYTICAL OR EDITORIAL COMMENT. STATEMENTS OR THEORIES ADVOCATED OR IMPLIED ARE THOSE OF THE SOURCE AND DO NOT NECESSARILY REFLECT THE POSITION OR OPINION OF THE FOREIGN TECHNOLOGY DIVISION.

PREPARED BY:

TRANSLATION DIVISION
FOREIGN TECHNOLOGY DIVISION
WPAFB, OHIO

Table of Contents

Graphics Disclaimer ii

Effect of Part Span Shroud on Performance of a Single Stage Compressor, by Duan Lianfeng, Dong Baochang, Wang Zhaolong 1

Effect of the Rear Stage Casing Treatment on the Overall Performance of a Multistage Axial-flow Compressor, by Gao Yaolin, Li Keming 18

Investigations on Performance of Swept Cascade of Axial Flow Compressor, by Yan Ruqum, Qian Zhaoyan 26

Thermal Performance of Turbine Vane with Ceramic Coatings and Enhanced Cooling, by Gu Weizao, Zhang Yuming 33

A-1

GRAPHICS DISCLAIMER

All figures, graphics, tables, equations, etc. merged into this translation were extracted from the best quality copy available.

EFFECT OF PART SPAN SHROUD IN PERFORMANCE OF A SINGLE STAGE COMPRESSOR *

Duan Lianfeng, Dong Baochang, Wang Zhaolong

(Shenyang Aeroenging Research Institute)

Abstract

Single stage compressors with and without part span shroud were designed and tested to investigate the effect of part span shroud on aerodynamic performance of the compressor. Test results indicated that the part span shroud effected not merely the local region adjacent to the shroud, but influenced almost all height of the annulus. Analysis indicated that the flow condition in the compressor is related to flow continuity equation and radial equilibrium equation. However the local disturbance caused by part span shroud not only results in radial re-equilibrium, but also causes the viscosity loss to increase and the elastic deformation at the blade tip resulted from centrifugal force to be prevented. This means that the effect of part span shroud spreads to all span. The local blockage and loss in region adjacent to the shroud should be considered in designing a compressor rotor with part span shroud. Thus, the effect of part span shroud on the flow field within the compressor could be included objectively in the design.

I. Introduction

For the aeroengine design of this date, the part span shroud usually is added on the compressor rotor such that the compressor

*This paper was presented at the Conference of Heat Engine Aerodynamic Thermodynamics held at Shamen, August 1981.

vibration can be prevented. Different methods, however, have been proposed to deal with the effect of part span shroud on the aerodynamic design. An experimental compressor, which is studied and analyzed approximately by a simple method called "equalizing the effect of part span shroud", is introduced in this paper. The idea of this method is that the rotor efficiency is reduced by 1～2% and the effect due to the blockage of part span shroud is corrected by increasing the correction coefficient at the attached layer, which is equally considered at the rotor's inlet and outlet calculation stations. This method may not truly represent the real aerodynamic behavior of the rotor with part span shroud, and whether this method can be applied to the pratical engineering is still not known because of the lack of practical experience. In this paper, we report the experimental results about the performance of a single stage compressor, with and without part span shroud on its first stage working blade, of a certain type of low pressure compressor which is designed by the method mentioned above. The observed effects of part span shroud on the aerodynamic performance of the compresor are also discussed in this paper.

II. Experimental Compressor

For the single stage compressor whose working blades do not have part span shroud, its rotor blade can be divided into two parts: ultrasonic first-half and surpass-sonic second-half. For the ultrasonic first-half, the relative Mach number at the inlet is 1.1 ～ 1.385; the middle section of the blade has an S-shape curvature and the surfaces of its basin and back are composed of straight lines and

hyperbolas; at the inlet, the surfaces of blade basin and blade back are straight lines; the surface of the rear section is composed of straight lines and hyperbola. For the surpass-sonic second-half, the curve of middle blade and the surfaces of blade basin and blade back are all hyperbolas. A BC-6 type blade is used as the stator.[11] A rotor without part span shroud is shown in Fig.1.

The single stage compressor whose working blades do have part span shroud is called a J223A single stage compressor. Its rotor blade is converted from the previous working blade without part span shroud by adding a "simple" part span shroud at the 55% designed flow line. The shapes of its stator and annulus are the same as that of the experimental compressor without part span shroud. The detail of its design can be found in Ref.2. The picture of J223A is shown in Fig.2.

The experiments were performed on the single and double stage compressor tester in our institute.

III. Experimental Results and Discussion

1. Experimental results and comparison of the general properties

The experimental data of the single stage compressor with part span shroud are quoted from Ref.3. The experimental data of the compressor without part span shroud are quoted from Ref.4. The measured general properties of the experimental compressors with and without part span shroud are plotted in Fig.3 for comparison. As can be seen from Fig.3, after the part span shroud is added on the rotor blade, its maximum flow rate is reduced by 1%; its maximum efficiency is reduced by 2%; and the maximum pressure ratio is reduced by 2.5%.

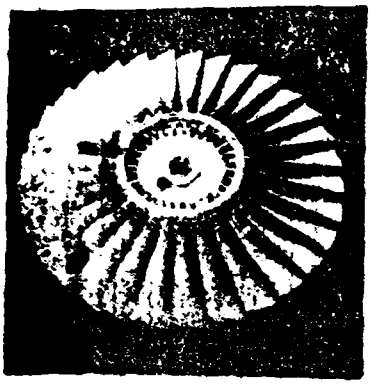

Fig.1. Rotor without part span shroud.

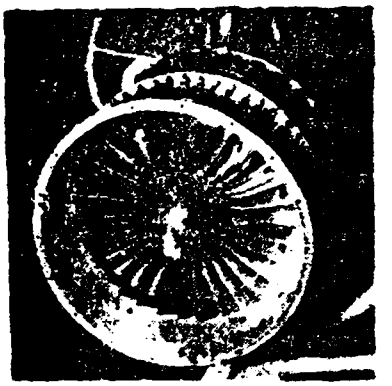

Fig.2. Compressor with part span shroud.

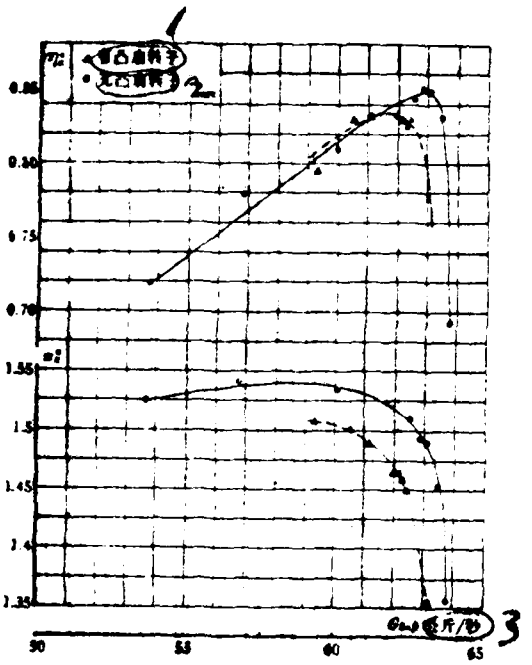

Fig.3. The general properties of single stage compressors with and without part span shroud. (1:rotor with part span shroud; 2:rotor without part span shroud; 3: Kg/sec)

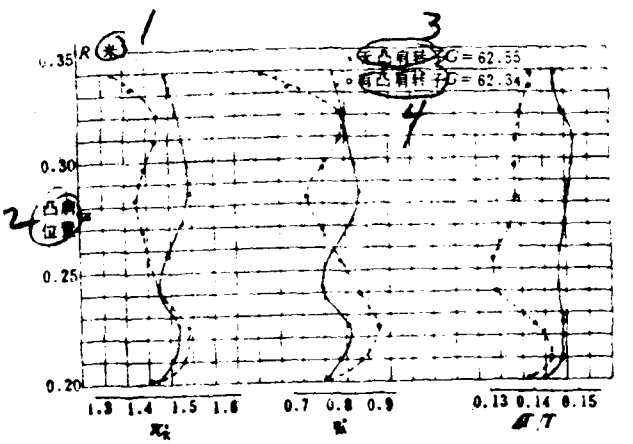

Fig.4. The effect of part span shroud on the performance of base element of single stage compressor. (1: m; 2:positio of part span shroud; 3:rotor without part span shroud; 4:rotor with part span shroud)

Their absolute values are listed in Table I.

Table I. The effect of part span shroud on general properties. (1: single stage compressor without part span shroud; 2: single stage compressor with part span shroud; 3: relative variation value; 4: Kg/sec; 5: note; 6: value with part span shroud; 7: value without part span shroud)

	$G_{Bo,max}$ (公斤/秒)	η^*_{max}	π^*_{max}	备注
1 无凸肩单级	63.76	0.849	1.539	
2 有凸肩单级	63.20	0.833	1.507	
3 相对变化值	−1%	−2%	−2.5%	相对变化值 = (有凸肩值 − 无凸肩值) / 无凸肩值

2. The effect of part span shroud on the property of base elements.

We compare two experiments whose flow rates are almost the same. Their general property parameters are listed in Table II.

Table II. General property parameters of two experiments with the same flow rate. (1: single stage compressor without part span shroud; 2: single stage compressor with part span shroud; 3: Kg/sec)

	G_{Bo}, (公斤/秒)	π^*	η^*
1 无凸肩单级	62.55	1.508	0.844
2 有凸肩单级	62.34	1.458	0.826

The effects of part span shroud on the property of a single stage compressor base element are shown in Fig.4. The effects of part span shroud on the property of a rotor base element are shown in Fig.5. It should be noted that the results in Fig.5 are calculated by a computer

using the measured data, where we assume $T_3^* = T_1^*$, $P_3^* = P_{3max}^*$ in the direction of flow line (same assumption and same computer program are employed both for the cases with and without part span shroud). For simplicity, this calculation does not consider the mixing due to radial flow at the stator blade which is resulted from the radial pressure gradient. For the rotor with part span shroud, the pressure gradient is bigger at the region adjacent to the outlet shroud. When air flows through the stator slot, the mixing due to radial flow becomes severe. If the above assumption is employed, then the calculated flow parameters of the rotor with part span shroud will have greater error than that of a rotor without part span shroud. The calculated property parameters at the outlet of the rotor also can not represent the real situation. But for qualitative analysis, this calculation is still applicable.

From Figs.4 and 5, we can see that:

a. After part span shroud is added, the flow lines of the air flow in the annulus of the rotor and stator shift to hub. The change of flow line distribution reflects the change of the flow field. So, the air flow must undertake radial re-equilibrium. According to the calculation results of Refs. 4 and 5, at the outlet of a blade without part span shroud, the first ring surface (the outlet ring surface is divided into ten parts) at the root allows 11.8% of total flow to pass through; the tenth ring surface at the tip allows 9.1% of total flow to pass through; and the sixth ring surface at the middle of the blade allows 10.2% of total flow to pass through. If the part span shroud is added to the rotor blade, then the air flow passing through the first ring surface at the root increases to 12.4%; the air flow

passing through the tenth ring surface at the tip increases to 7.5%; and the air flow passing through the sixth ring surface (approximately at the position where the part span shroud locates of the blade is 9.8%. The re-distribution of the flow rate will cause the property of the base element change.

b. After the part span shroud is added, the work augmentation is reduced for all span. The absolute values of work augmentation for all span are listed in Table III.

Table III. The change of work augmentation in the span direction. (1: single stage compressor without part span shroud; 2: single stage compressor with part span shroud; 3: relative variation value; 4: root; 5:flow line; 6:middle; 7:tip; 8:note; 9:value with part span shroud; 10:value without part span shroud)

4	6	7	
$\Delta T^*/T_1^*$	根部 (15% 流线处) 5	中部 (55% 流线处) 5	尖部 (85% 流线处) 5	备 注 8
1 无凸肩单级	0.1465	0.1479	0.1464	
2 有凸肩单级	0.1403	0.1365	0.1373	9 10
3 相对变化值	−4.2%	−7.7%	−6.2%	相对变化值 = 有凸肩值 − 无凸肩值 / 无凸肩值 10

The change of work augmentation is mainly due to the following two causes: the first one is that the part span shroud at the 55% designed flow line of the rotor will restrict the elastic deformation resulting from centrifugal force, which will reduce the value of C_{u_2} and then reduce the work augmentation; the second one is that the part span shroud will change the radial equilibrium of the air flow, which also forces the change of work augmentation.

c. Part span shroud affects the efficiency of the base element for all span. The efficiency of one third of the blade, which is around

the part span shroud, decreases because of the influence of shroud. In other words, the range affected by part span shroud is about 11 times of the thickness of shroud (~4mm). The maximum efficiency is reduced by 11%, and the average efficiency is reduced by 5%. For the other one third of the blade, which is around the hub, the efficiency is improved. The efficiency of the base element is increased by 5 ~ 8%.

d. Since work augmentation and efficiency change, the pressure ratio will also change. The pressure ratios of the base element with and without part span shroud are listed in Table IV.

Table IV. The effect of part span shroud on the pressure ratio of the base element. (1:single stage compressor without part span shroud; 2:single stage compressor with part span shroud; 3:relative variation value; 4:root; 5:flow rate; 6:middle; 7:tip; 8:note; 9:value with part span shroud; 10:value without part span shroud)

1	根部 (15% 流线处) 4	中部 (55% 流线处) 6	尖部 (85% 流线处) 7	备 注 8
无凸肩单级	1.495	1.52	1.491	
2 有凸肩单级	1.515	1.40	1.447	9
3 相对变化值	1.3%	−7.9%	−3%	相对变化值 = (有凸肩值 − 无凸肩值) / 无凸肩值 10

3. The effect of part span shroud on the radial distribution of flow parameters at the inlet and outlet of the motor.

Since there is no direct measurement at the outlet of the rotor, the inlet and outlet flow fields of various blades are estimated by using the measured values of the single stage compressor at the inlet and outlet and by using the "flow field calculation (S_2) program". In the calculation, the effect of part span shroud is considered by the

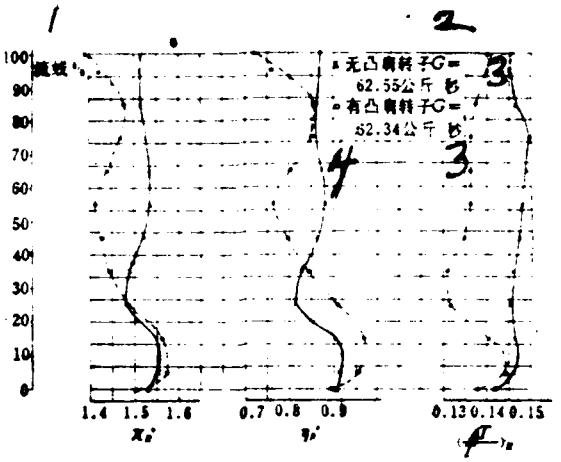

Fig.5. The effect of part span shroud on the performance of rotor base element. (1:flow line; 2:rotor without part span shroud; 3:Kg/sec; 4:rotor with part span shroud)

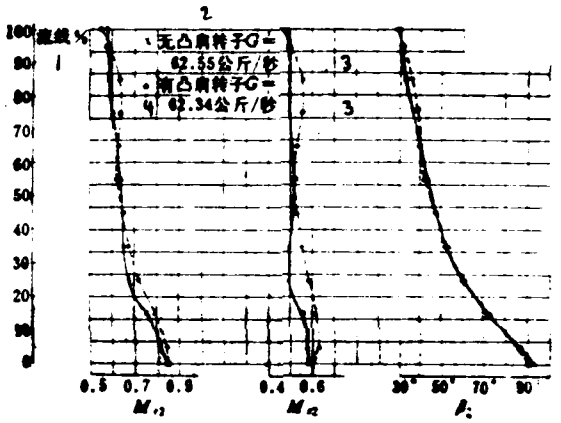

Fig.6(a) Radial distribution of flow parameters at the outlet of rotor. (1: flow line; 2:rotor without part span shroud; 3:Kg/sec; 4:rotor with part span shroud)

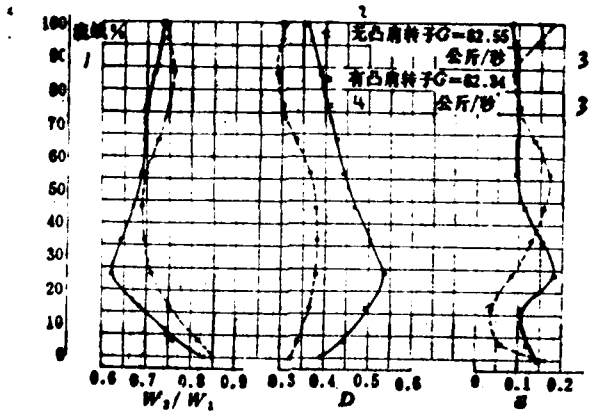

Fig. 6(b) Radial distribution of flow parameters at the outlet of rotor. (1: flow line; 2: rotor without part span shroud; 3: Kg/sec; 4: rotor with part span shroud)

conventional method, namely, the blockage effect of part span shroud is considered equally. The blockage value at the rotor inlet is added by half of the blockage value at the windward area of the shroud. The blockage value of the rotor outlet is added by one while blockage value at the windward area of the shroud. Although this may not represent the real air flow behavior in the rotor with part span shroud, but approximately it is still applicable for the analysis of the problem.

According to the analysis of the experimental data, the effect of part span shroud on the flow field at the rotor inlet is very small.

The radial distributions of flow parameter at the inlet and outlet of the rotor areshown in Fig.6. As can be seen from Fig.6, the elastic deformation of the rotor blade is restricted by the part span shroud such that the work augmentation is reduced. The average axial velocity of air flow coming out from the rotor is faster than that of the rotor without part span shroud. The velocity ratio W_2/W_1 also increases. So in general, the rotor load is reduced (the diffusion factor D is reduced by 0.05 ~ 0.1). But at the region around part span shroud, due to the blockage and disturbance of part span shroud, the local axial velocity becomes smaller. The axial velocity M_{z_2} at that region is very close to the velocity without part span shroud. Because of this, the axial velocity at the regions of hub and tip will increase correspondingly. The flow field inside the rotor annulus will thus re-distribute and cause the flow lines to shift downward. As shown in Fig.6 (b), at the one third of the blade adjacent to the hub of the rotor without part span shroud, the rotor load is larger and the efficiency is lower. If part span shroud is added, due to the

increase of flow rate around the hub, the rotor load decreases (D value is reduced from 0.535 to 0.389) and then the efficiency at the root of the rotor is improved. This means that the part span shroud influences almost all height of the rotor annulus. Whenever the radial equilibrium of air flow in the rotor annulus changes, the rotor property will also change. Therefore, the local blockage adjacent to part span shroud should be considered in the calculation of the flow field such that the calculation can be better applied to the real situation.

As can be seen from Fig.6, the pressure ratio at the root region is improved. As an example, the pressure ratio at 15% flow line is increased from 1.546 to 1.562. This is because the loss is reduced. Due to the effect of part span shroud, at the 35～70% flow line adjacent to the part span shroud, the work augmentation decreases and the loss increases such that the total pressure ratio decreases greatly. As an example, the total pressure ratio at 55% flow line is reduced from 1.536 to 1.415 and the relative variation value is 8%. This bad performance area is about one third of all span and is about 10 times of the thickness of part span shroud. At the 75～90% flow line adjacent to the rotor tip, the inlet and outlet velocity ratio W_2/W_1 increases and the rotor load decreases. But according to the previous experimental results, under the condition that diffusion factor $D<0.4$, the total pressure loss parameter does not show a decrease clearly with decreasing D value. Since the elastic deformation of the blade is restricted by part span shroud, the work augmentation is much less than that without part span shroud and the rotor pressure ratio is also less than that without part span shroud. As an example, at the

95% flow line region, the total pressure ratio is reduced from 1.42 to 1.47. At the 95% flow line adjacent to the blade tip, the loss increases. This can be explained as below. After part span shroud is added, the elastic deformation of the blade is small. Its stagger angle is about -3°. On the other hand, if the part span shroud is not added, the elastic deformation of the blade under the centrifugal force will increase the stagger angle at the blade tipby 2 ~ 3°. This implies that the blade tip is working under 0° stagger angle. It is obvious that working under a negative stagger angle is worse than working under 0° stagger angle. So, the loss will increase after the part span shroud is added.

4. The effect of part span shroud on the flow parameters at the inlet and outlet of the stator

The radial distribution of flow parameter at the inlet of the stator is shown in Fig.7. The radial distribution of flow parameter at the outlet of the stator is shown in Fig.8. The effect of part span shroud on the inlet stagger angle of the stator is shown in Fig.9.

As can be seen from the figures, both the inlet Mach number and the inlet stagger angle of the stator have distinct changes after part span shroud is added. At the one third of span which is adjacent to the hub, the value of M_{c3} increases by 0.03 ~ 0.05. The diffusion factor of the stator decreases by 0.05 ~ 0.1. The stator stagger angle, in general, is reduced by 2 ~ 6° for all span. The stator of our experimental compressor is the model of BC-6. Without part span shroud, the values of M_{c3} and D_s are not too big (at root region, M_{c3} = 0.65 ~ 0.82, D_s = 0.33 ~ 0.38). So, after the part span shroud is added to the rotor, the stator still can adapt itself to this change.

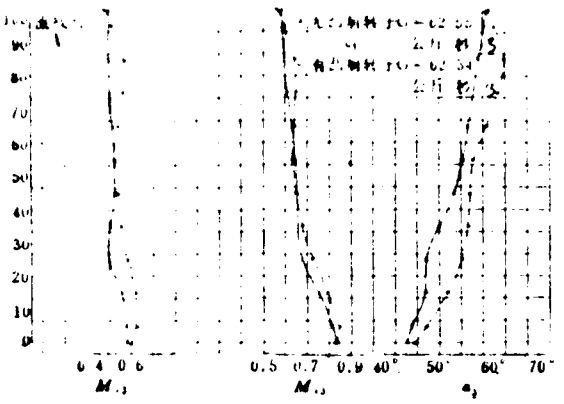

Fig.2. Radial distribution of flow parameters at the inlet of stator. (1: flow line; 2: rotor without part span shroud; 3: Kg/sec; 4: rotor with part span shroud)

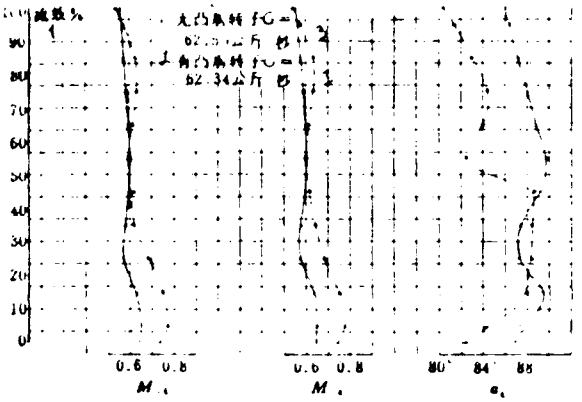

Fig. 3(a) Radial distribution of flow parameters at the outlet of stator. (1: flow line; 2: rotor without part span shroud; 3: Kg/sec; 4: rotor with part span shroud)

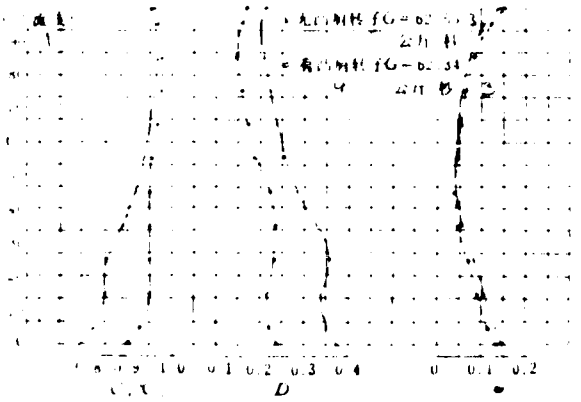

Fig. 3(b) Radial distribution of flow parameters at the outlet of stator. (1: flow line; 2: rotor without part span shroud; 3: Kg/sec; 4: rotor with part span shroud)

There is no obvious change for the use of the stator. This primarily is one of the reasons why the surpass-sonic rotor has to be combined with the sub-sonic stator.

The change of flow line position after part span shroud is added is shown in Fig.10. This figure shows that part span shroud changes the flow parameter distribution of the whole flow field. All the flow lines shift downward more or less. The farther from the part span shroud it is, the smaller the effect is. In general, the air flow at the region between part span shroud and the hub is affected more, and the air flow at the region between part span shroud and the tip is affected less. This is consistent with the experimental results reported in the other countries.

IV. Conclusion

1. Comparing the results of single stage compressor without part span shroud, the part span shroud reduces the maximum flow rate by 1%, the maximum efficiency by 2%, and the maximum pressure ratio by about 2.5%.

2. The effect of part span shroud on the areodynamic performance of a compressor is not restricted to a local region. The effect spreads almost to all span. This is because the flow condition in the compressor is related to the flow continuity and radial equilibrium equation. The local disturbance caused by part span shroud not only results in radial re-equilibrium, but also causes the viscosity loss to increase and the elastic deformation at the blade tip to be prevented.

3. To design the rotor with part span shroud, the effect of part span shroud on the radial distribution of efficiency should be

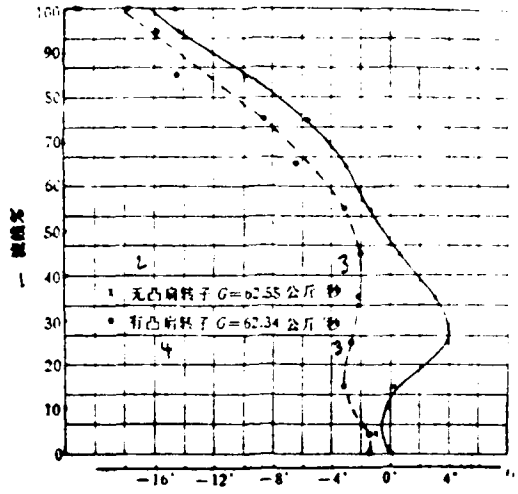

Fig. 9. The effect of part span shroud on the inlet stagger angle of stator. (1: flow line; 2: rotor without part span shroud; 3: Kg/sec; 4: rotor with part span shroud)

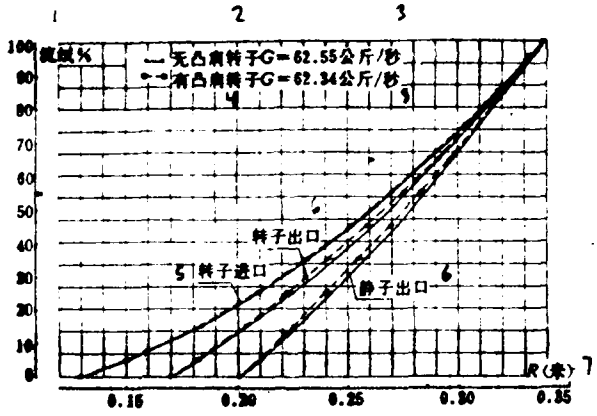

Fig. 10. The change of flow line position after part span shroud is added. (1: flow line; 2: rotor without part span shroud; 3: Kg/sec; 4: rotor with part span shroud; 5: rotor outlet; 6: rotor inlet; 7: m)

considered. It is better to use the method of "loss localization" than to use the method of "loss equalization" for the design of the compressor with part span shroud.

4. The local blockage and loss in the region adjacent to the shroud should be considered in designing a compressor rotor with part span shroud. In other words, the existence of part span shroud should be considered in calculation of a flow field. We call this method "localization of blocking shroud". By this way, the effect of part span shroud on the change of flow field distribution can be truly reflected.

5. The inlet Mach number of the stator should be as small as possible in designing a compressor rotor. It is better to use a sub-sonic blade such that the adaptability of the stator to the change of air flow can be enhanced.

Finally, the authors wish to thank colleagues Wei Yubing and Chen Baoshi for their technical assistance.

References:

[1] Liu shugu, "The manual for the design of a certain single stage experimental compressor", progress report of Shenyang Aeroenging Research Institute, 1962.

[2] Zhang Tianyi, "The design of a certain double stage aerodynamic fan", progress report of Shenyang Aeroenging Research Institute, 1976.

[3] Duan Lianfeng, "The first conclusion of the first test for a certain double stage fan ", progress report of Shenyang Aeroenging Research Institute, 1980.

[4] Duan Lianfeng, "The first test report of a certain II type compressor", progress report of Shenyang Aeroenging Resesarch Institute, 1978.

Effect of the Rear Stage Casing Treatment on the Overall Performance of a Multistage Axial-flow Compressor *

Gao Yaolin

(Shenyang Aeroengine Company

Li Keming

(Shenyang Aeroengine Research Institute)

ABSTRACT

A trouble shooting test progress report on "C" compressor is presented. It mainly describes the test results concerning the effects of casing treatment and varying the stagger angle of the rotor blades at stages 7, 8, and 9 on the overall performance of a multistage axial-flow compressor. The test results show that the casing treatment of the rear stages is a very effective method to extend the stable operating range of the compressor at high speeds.

I. The Origin of Test and the Choice of Program

After a "C" compressor, which is converted from the prototype compressor, is mounted on a certain type of engine, a stall breakdown occurs at high altitude after successive thrust augmentation. According to the measurements in the relevant test flight, this stall is caused by the gasp vibration in the compressor. When stall occurs, the speed of the compressor $\bar{n}$ is in the range of $1.03 \sim 1.08$. In order to fully understand the mechanism of this stall breakdown and to find out the solution of this problem, it is necessary to perform some tests on the performances of the relevant compressors.

There are five compressors which are under testing.

*This paper was presented at the Conference of Heat Engine Aerodynamic Thermodynamics held at Shamen, August 1981.

1. Prototype compressor (for simplicity, we call this compressor I): This is the nine stages axial-flow compressor whose first stage is surpass-sonic.

2. "C" compressor (or compressor II): The only difference between this compressor and compressor I is that they have different rear cabin structures.

3. "Twist blade" compressor (or compressor III): This compressor is converted from compressor II, where the stagger angles of blade tips for the rotors of the last few stages are reduced by 1 ~ 2°. The stagger angles of the blade root remain the same, and the stagger angles between the tip and root are varied according to a certain natural regularity.

4. Casing treatment compressor (or compressor IV): This compressor is converted from compressor II, where the exteriors of the seventh and ninth rotors are treated by ring slot casing treatment (see Fig.1)

5. "Twist blade" and "casing treatment" compressor (or compressor V): This compressor is converted from compressor II, where both the treatments of "twist blade" and "casing treatment" are employed.

II. Testing Results and Analysis

The seven equal speed contours, $\bar{n}$= 0.7, 0.8, 0.9, 0.95, 1.0, 1.05, 1.10, of the above five compressors are measured while the outgas valve is closed. The data of $\bar{n}$=1.05 and 0.95 are missing for compressors III and IV. These experiments were cancelled at that moment because of the reason for safety. When we tested the gasp

vibration of compressor IV as $\bar{n}$=1.15, we observed a very special phenomenon where "superhigh temperature developed in the compressor during gasp vibration".[1] When this phenomenon occurred, the blade tips about one third of the blade height of the rotors from the second to fifth stages were all melted within a few seconds. So, the test of this compressor as $\bar{n}$ = 1.10 was not performed.

Since we have a lot of experimental data, in order to have a better understanding and clear comparison, only the data around the gasp vibration for each compressor are plotted in Fig.2. Some of the equal speed contours are also plotted in Fig.2. The comparisons of the gasp vibration allowances and the efficiencies for each compressor are described below in more detail.

1. Comparison of the gasp vibration allowance

The variations of the gasp vibration allowance for each compressor, while the engine is operating under the "specified" and "augmented" conditions, are shown in Fig.3.

As can be seen from Fig.3, in the range of $\bar{n}$=0.7～0.5, the gasp vibration allowance of compressor II is higher than that of compressor I. This is consistent with the observation in the test engine that the "speed of the upper boundary of gasp vibration" is reduced. When $\bar{n}$ > 0.8, however, the allowance loss of gasp vibration in compressor II increases with increasing the speed. In the "specified" state, when $\bar{n}$=0.9～1.10, the allowance loss is 2.6～8.4% and the relative loss is 12～36%; in the "Augmented" state, when $\bar{n}$=0.95～1.10, the allowance loss is 3.2～7.9% and the relative loss is 18～44%. When high altitude stall occurs, the engine speed $\bar{n}$ is in the range of 1.03～1.08. At this range, the reduction of the gasp vibration allowance

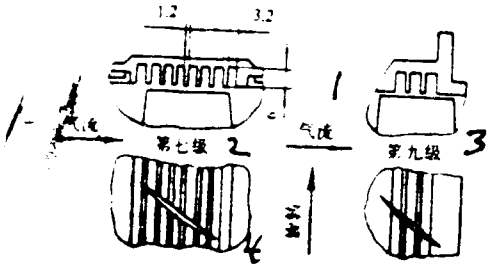

Fig.1. Ring slot casing treatment on the exterior of rotor. (1:air flow; 2:7th stage; 3:9th stage; 4: rotation)

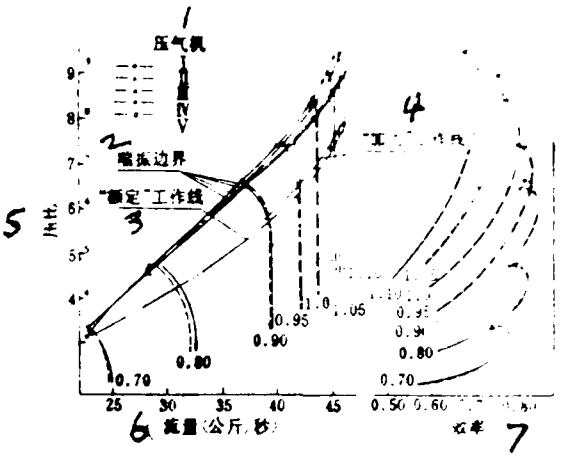

Fig.2. Some characteristics of various compressors. (1:compressor; 2:boundary of gasp vibration; 3:"specified" operating line; 4:"augmented" operating line; 5:pressure ratio; 6:flow rate (Kg/sec); 7:efficiency)

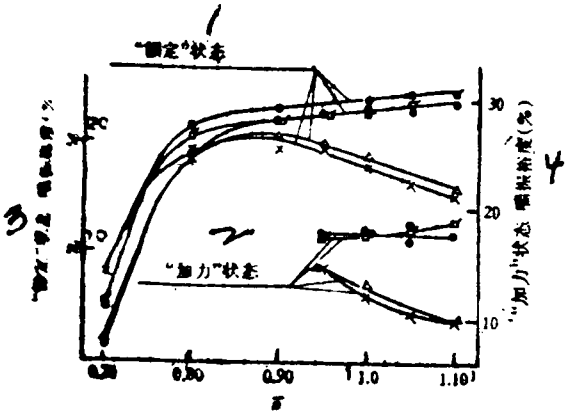

Fig.3. The gasp vibration allowance of various compressors. (1:"specified" state; 2:"augmented" state; 3:gasp vibration allowance of "specified" state; 4: gasp vibration allowance of "augmented" state)

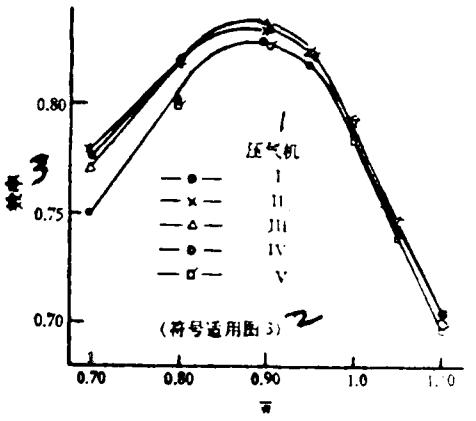

Fig.4. The operating point efficiency of various compressors. (1:compressor; 2:these symbols are also applied to Fig.3 ; 3:efficiency)

for compressor II is minimum.

In contrast to compressor II, compressor III, which has a smaller stagger angle due to the twisting of rotor blades in the last few stages, has a longer time before stall occurs and has a higher vibration allowance. But the reduction of stagger angle will make the work augmentation smaller. So, the overall vibration allowance of compressor III does not increase as much as compressor II. As an example, in the "augmented" state and $\bar{n}$ = 1.0, the allowance only increases 1.1% and the relative increment is 9 %. It should be noted that the twisting of the rotor blade will cause the characteristic lines to shift to the position with less flow rate. Although the gasp pressure ratio is reduced, the reduction of flow rate will lower the operating point. Considering all these effects, the gasp vibration allowance is only enhanced slightly.

After casing treatment is performed in the 7th and 9th stages, both compressors IV and V have bigger gasp vibration allowances, especially in the designed high speed range, than compressor II. In the "specified" state, when $\bar{n}$ = 0.95 ~ 1.10, compressor V has an allowance increase of 2.8 ~ 9.1% and relative increment 14 ~ 60%; in the "augmented" state, its allowance increases 2.8 ~ 9% and its relative increment is 19 ~ 90%. In general, the stable operating range of compressor V is slightly larger than that of compressor I. If only the casing treatment is employed (i.e., compressor IV), the result is even better. Although the data of $\bar{n}$ = 1.10 is missing in this compressor, from the trend of the data of the other speeds, it shows that the gasp vibration allowance of compressor IV is better than that of compressor I.

The results of casing treatment also can be seen from Fig. . Comparing compressor V with compressor III, at $\bar{n}$ = 1.0 ~ 1.1, the former's gasp vibration allowance is 4 ~ 8.8% higher than that of the latter and the relative increment is 22 ~ 57% in the "specified" state; in the "augmented" state, the former's allowance increases 4.6 ~ 7.9% and the relative increment is 35 ~ 80%. Comparing compressor IV with compressor II, in the "specified" state, the former's allowance increases 6.4 ~ 9.5% (estimated) and the relative increment is 37 ~ 63%; in the "augmented" state, the former's allowance increases 5.8 ~ 9.2% (estimated) and the relative increment is 49 ~ 94%.

In Fig. 2, if we compare the gasp vibration boundaries of each compressor very carefully, then we will find a common regularity: It does not matter if it is a casing treatment compressor or a solid casing compressor; their stage loads are reduced due to the twisting of the rear stage rotor blades. Because of this, their gasp pressure ratios also decrease. But the gasp pressure ratio of the casing treatment compressor is higher. A very important requirement for the casing treatment thus can be obtained: The effect of casing treatment is most obvious if the treatment is performed on the stage where the stage load is largest and the stall is easier to occur.

2. Comparison of the compressor's efficiency

The efficiency of the operating point in the "specified" state vs the compressor speed is shown in Fig. 4. As can be seen from this figure, for all speed ranges, the operating point efficiency of compressor II is close to or slightly higher than that of compressor I. So from the point of view of efficiency, changing the rear cabin structure is good for compressor II. The efficiency of compressor III

is almost the same as that of compressor II. This indicates that the twist blade has little effect on the operating point efficiency. But for compressor V which is treated both by casing treatment and the twist blade, its operating point efficiency is slightly lower than that of compressor III which is only treated by the twist blade. The efficiency is only reduced 0.8% in the range of $\bar{n} = 1.0 \sim 1.10$. The operating point efficiency of compressor IV with casing treatment is almost the same as that of the compressor with solid casing.

III. Conclusion

1. An appropriate rear stage casing treatment on the multistage axial-flow compressor can enhance the gasp vibration allowance effectively at a high speed range.

2. For the compressor without twisting the rotor blades in the rear stage, the casing treatment almost does not have any effect on its efficiency. But for a compressor with a twisting rotor blade, the casing treatment lowers its efficiency for all speed ranges.

3. The inlet stage casing treatment on a multistage axial-flow compressor is mainly used to improve its ability of distortion resistance and its performances at middle and low speeds. The rear stage casing treatment, however, is mainly used to improve its gasp vibration allowance at high speeds (especially at ultra high speed). It should be pointed out that not only the type of structure and parameter [2] need to be considered in the casing treatment of a multistage compressor, different stages and parts have to be selected for different compressors.

4. The reason why "C" compressor stalls at high altitude is that

the change of the static blade structure from the 6th to 8th stage worsens the operating condition for the rear stage rotor.

5. From our experimental results in this paper, we have the following proposal. By combining the techniques of inlet stage and rear stage casing treatments, it is possible to design a compressor which has high gasp vibration allowance at all speeds and also has acceptable efficiency. Right now, this proposal is under investigation by our group.

Liu Peichen, Yang Qianhu, Jin Baofu, and Zhou Gong also participated in this project. The authors wish to thank the colleagues in the Third Research Laboratory of Shenyang Aeroengine Research Institute for their technical assistance and support.

References

[1] Gao Yaolin, "The phenomenon of high temperature gasp vibration in a compressor", progress report of Shenyang Aeroengine Company, 1JZ1381,1980

[2] Roger W. Snyder and Robert J. Blade: Analytical Study of Effect of Casing Treatment on Performance of a Multistage Compressor, NASA TN D-6917, 1972

Investigations in Performance of Swept Cascade of Axial Flow Compressor *

Yan Ruqum and Qian Zhaoyan

(North-Western Polytechnical University)

ABSTRACT

The aerodynamic performances of swept-cascade of axial-flow compressor are researched in this paper, and the calculating methods of coefficient of total pressure losses, critical Mach number and turning angle of swept cascade are provided. The flow features on swept blade along span direction are also studied, the average wake contours and experimental data of various locations in span direction at given operating condition are presented.

I. Calculation on the Performance of Swept Cascade of Compressor

Critical Mach number M_{kp}: According to the swept-back wing theory of the aircraft, the critical Mach number of the swept cascade can be obtained by the following equation:

$$(M_{kp\cdot\lambda}/M_{kp\cdot 0}) = (V_\lambda/V_0) = \cos\lambda$$
$$M_{kp\cdot 0} = M_{kp\cdot\lambda}/\cos\lambda \tag{1}$$

where $V_{\bar{0}}$ and $V_{\bar{\lambda}}$ represent the flow velocities of the vertical cascade (sweep angle $\lambda = 0$) and the swept cascade (sweep angle is λ) of the same type of blade. So, by comparing with the vertical cascade, the increase of the critical Mach number of the swept cascade is:

$$\Delta M_{kp} = M_{kp\cdot\lambda}[(1/\cos\lambda) - 1] \tag{2}$$

Total pressure loss of the swept cascade: According to Eq. (2),

*This paper was presented at the Conference of Heat Engine Aerodynamic Thermodynamics held at Shamen, August 1981.

we have

$$\Delta M_1 = M_{1\cdot x}[(1/\cos\lambda) - 1] \tag{3}$$

According to Ref. 1, at a certain cascade inlet Mach number M_1, the total pressure loss coefficient $\bar{\omega}$ of the vertical cascade of axial-flow compressor is:

$$\omega_x = \tilde{M}_1(\sin\beta_1/\sin\beta_2)^2\bar{\theta}_2(1-\bar{\theta}_2H_2)^{-3} \cdot 4H_2/(3H_2-1) \tag{4}$$

where $\tilde{M}_1 = f(M_1)$ is called the cascade inlet Mach number parameter (its relation with M_1 is shown in Fig. 1); $\bar{\theta}_2 = (\theta_2/b)\times(\sigma/\sin\beta_2)$ is the momentum parameter of the attached surface layer; $\sigma = b/t$ is the cascade density; and $H_2 = \delta^*/\theta_2$ is the shape factor.

Comparing with the vertical cascade, the increment of inlet Mach number M_1 of the swept cascade (ΔM_1) is smaller. Let's assume (1) in these two cases, the flow parameters β_1 and β_2 and the characteristic parameters of the primary attached layer $\bar{\theta}_2$、θ_2、H_2, etc do not change much; (2) $\tilde{M}_{1\cdot n}/\tilde{M}_{1\cdot x} = M_{1\cdot x}/M_{1\cdot n}$. The latter assumption is almost correct for each point of the $\tilde{M}_1 \sim M_1$ curve in Fig. 1. According to these two assumptions, we have the following equations:

$$\omega_n = \tilde{M}_{1\cdot n}(\sin\beta_1/\sin\beta_2)^2\bar{\theta}_2(1-\bar{\theta}_2H_2)^{-3} \cdot 4H_2/(3H_2-1) \tag{5}$$

and

$$\tilde{M}_{1\cdot n} = \tilde{M}_{1\cdot x} \cdot M_{1\cdot x}/M_{1\cdot n} \tag{6}$$

If Eq. (3) is considered, after some calculations, we have

$$\tilde{M}_{1\cdot n} = \tilde{M}_{1\cdot x}\cos\lambda \tag{7}$$

Substituting Eq. (7) into Eq. (5), then we have

$$\omega_n = \tilde{M}_{1\cdot x} \cdot \cos\lambda \cdot (\sin\beta_1/\sin\beta_2)^2\bar{\theta}_2(1-\bar{\theta}_2H_2)^{-3} \cdot 4H_2/(3H_2-1) \tag{8}$$

Therefore, the $\bar{\omega}$ value of the compressor's swept cascade (sweep angle is λ) can be calculated by Eq. (8).

According to Ref. 2., the backward angle δ of the compressor's swept cascade still can be calculated by the Carter's formula.

Besides, according to the swept-back wing theory of the aircraft, the following equation is true for the compressor's swept cascade and the corresponding vertical cascade.

$$\tan\alpha_{\lambda} = \tan\alpha_{\lambda}/\cos\lambda \tag{9}$$

where α is the incoming flow angle before the cascade. Since $\alpha = \gamma - \beta_1$, the gas inlet angle of the swept cascade is

$$\beta_{1\cdot\lambda} = \gamma - \tan^{-1}[\tan^{-1}(\gamma - \beta_{1\cdot\lambda})/\cos\lambda] \tag{10}$$

So, under a given operating condition, the flow turning angle $(\Delta\beta)_{\lambda}$ of the compressor's swept cascade should be

$$(\Delta\beta)_{\lambda} = \beta_{2\gamma\cdot\lambda} - \{\gamma - \tan^{-1}[\tan^{-1}(\gamma - \beta_{1\cdot\lambda})/\cos\lambda]\} \tag{11}$$

where γ is the stagger angle of the blade; $\beta_{1\cdot\lambda}$ is the corresponding gas inlet angle of the vertical cascade; $\beta_{2\gamma\cdot\lambda}$ is the average gas outlet angle of the swept cascade.

II. Experimental Investigation on the Swept Cascade of Compressor

The wind tunnel experiment of the compressor with swept cascade was performed in the subsonic plane cascade wind tunnel of North Western Polytechnical University. For the details about the structure and performance of this tunnel, the geometry parameters of the swept cascade of this axial-flow compressor, and the automatic measuring system and the automatic recording system of this wind tunnel can be found in Refs. 1-3. A series of wind tunnel experiments had been performed on the swept cascade with various inlet Mach numbers M_1 and various gas inlet angles. Comparing the measured total pressure loss coefficient and gas outlet angle (or backward angle δ) of the swept

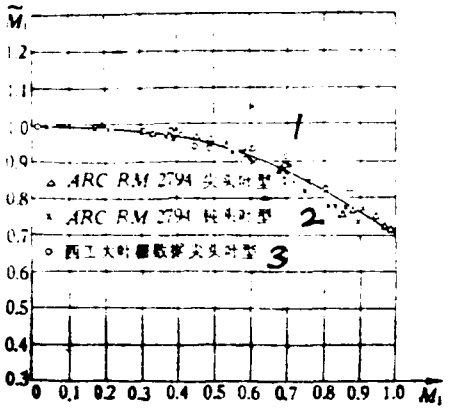

Fig.1. The inlet Mach number parameter $\tilde{M}_1$ of the vertical cascade compressor vs its inlet Mach number M_1. (1: blade with sharp tip; 2: blade with blunt tip; 3: sharp tip cascade data measured by North Western Polytechnical University)

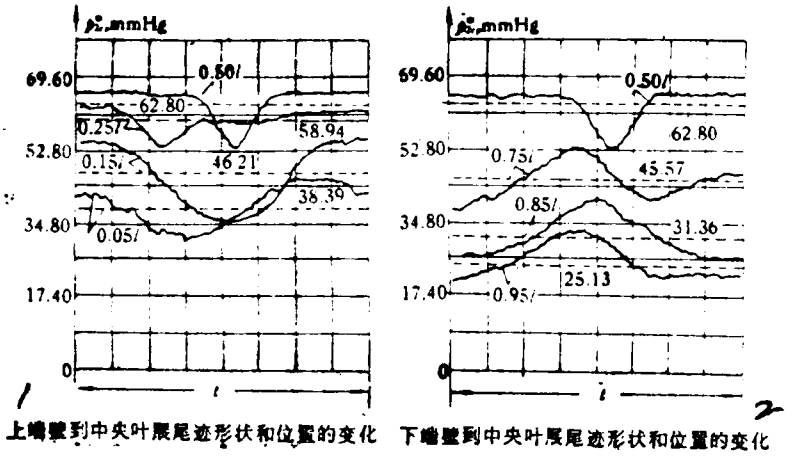

Fig.2. The change of total pressure after cascade P_2^*, wake contour and position at various locations in span direction from upper wall to bottom wall of the swept cascade of compressor. (1: the change of wake contour and position from the upper wall to the middle of span; 2: the change of wake contour and position from the bottom wall to the middle of span)

cascade with the corresponding theoretical values calculated by Eqs. 1 and 3, the agreement is very good.

The distributions of the total pressure P_2^* after cascade and the gas outlet angle β_2^*, in the wake contours of the compressor with swept cascade, are measured at the outlet measuring station 0.6 b from the rear edge of cascade for various locations in span direction from the upper end wall to the bottom end wall. On the other hand, the total pressure P_{2cp}^*, total pressure loss Δp^*, and the total pressure loss coefficient $\bar{\omega}$ are calculated at the corresponding locations in span direction. The variations of these parameters along the span direction are shown in Figs. 2 and 3, respectively. During the wind experiment, the inlet flow Mach number M_1 before the cascade is 0.44.

On the adsorption surface of the swept blade, the low energy gas molecules in the attached layer can move along the span direction. The moving direction is from the location, where the leading edge of the swept blade and the end wall form an abtuse angle, to the location, where the leading edge of the swept blade and the end wall form an acute angle. In the wind tunnel experiment where $M_1 = 0.44$, the total pressure loss Δp^* and the total pressure loss coefficient $\bar{\omega}$ of the upper wall are about 50% higher than those of the bottom wall. When the inlet flow Mach number M_1 is increased from 0.44 to 0.8, according to the calculation, the total pressure loss coefficient $\bar{\omega}$ at the bottom wall is twice as much as that at the upper wall.

References

[1] Yan Ruqum and Qian Zhaoyan, "Theoretical analysis and experimental

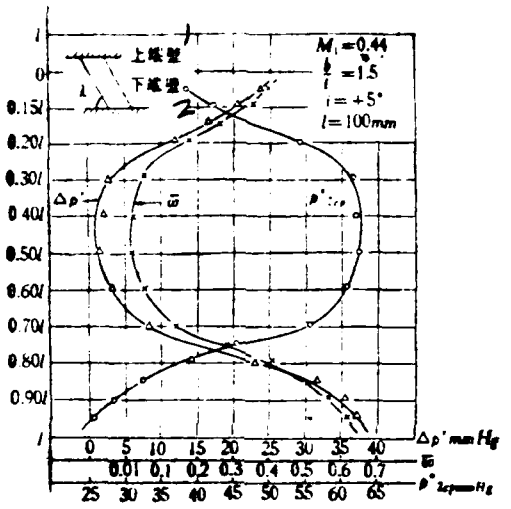

Fig. 3. The change of total pressure loss Δp^* of the oblique blade, total pressure p_2 after cascade, and the total pressure loss coefficient $\bar{\omega}$ in the span direction. (1: upper wall; 2: bottom wall)

investigation [illegible] high [illegible]", J. Engineering Thermophy. 2, 1 1981).

[2] Cascade experiment group, "Experimental investigation on the plane cascade and the judgment of the effect of sweeping back", Scientific and technical report of North Western Polytechnical University, 114 (1978).

[3] Qian Zhaoyan, "Automatical recording and manipulation on the experimental data of plane cascade in wind tunnel", Scientific and technical report of North Western Polytechnical University, 1976 (1979).

Thermal Performance of Turbine Vane with Ceramic Coatings and Enhanced Cooling*

Gu Weizao and Zhang Yuming

Institute of Engineering Thermophysics, Academia Sinica

ABSTRACT

Although ceramic coatings are remarkably heat-resistant, internal cooling for a high temperature turbine must still be enhanced in virtue of the limiting temperature of the alloy bond coat. Analysis carried out in this paper shows that the ceramic coating effectiveness is lower for a leading edge than for a flat section of the turbine vane and reduces with an increase in ceramic coating thickness. It strongly depends upon the cooling intensity of the turbine vane, and for this reason several ways of heat transfer augmentation in the turbine cooling passage are suggested. The relevant perameters of the first stage guided vane of a SPEY MK202 engine are used to calculate the temperature of the ceramic coatings. Calculations show that the thermal performance of the turbine vane is satisfactory and encouraging.

List of Primary Symbols

A radiation absorption coefficient

C Stephen- Boltzmann constant

de hydropower eguivalent diameter

F heat transfer area of the cooling passage in turbine vane

G flow rate of the cooling air

h, h^+ height of the rough rib, dimensionless height

Symbols of subscript

b bond coat

c heat transfer by cooling air or convection

f flame

g gas

m material of turbine vane

r roughened surface

*This paper was presented in the Heat Transfer Material Conference held at Huangshan, October, 1981.

R arc radius of the various layers in the leading edge of turbine vane

S node spacing of rough rib or disturbing column

T temperature

U perimeter

α convection heat transfer coefficient

δ thickness of various layers in turbine vane with ceramic coating

λ heat conduction coefficient

ε radiation coefficient

s smooth surface

w cool inner wall of turbine vane

0 leading edge of vane or ceramic surface

1 boundary surface between ceramic and bond coat

2 boundary surface between bond coat and vane

3 inner wall of vane

Increasing the gas inlet temperature not only can improve the properties of the aeroengine, but also can increase the thermal efficiency of the dynamic gas turbine. But the higher the inlet gas temperature of the turbine is, the higher the cooling requirement of the turbine vane. Too much cooling air and too complicated vane structure will largely reduce the benefit due to the high inlet gas temperature. Therefore, a new method for cooling the turbine vane is needed. The best way is, obviously, to use a high temperature resistant and high pressure resistant ceramic, which does not require cooling, as the material of the turbine vane. But unfortunately, this kind of high quality ceramic material is not available now and further investigation is still underway. On the other hand, however, an air cooled turbine vane with ceramic coating is proposed. This design can increase the heat resistance between gas and turbine vane such that a higher gas inlet temperature can be tolerated. It was shown by experiments [1] that a

zirconite ceramic could tolerate a temperature higher than 2273 K and was not damaged after 2000 times of heat circulation tests in the temperature range of 2273 K-300 K. The only problem is that the temperature at bond coat can not exceed 1367 K [2,3]. This requirement can be achieved by limiting the gas inlet temperature, choosing an appropriate ceramic coating thickness, and using necessary internal cooling intensity for the turbine vane. In this paper, by theoretical calculation, we will analyse and study the interelationship between these three factors and find out the thermal performance of this turbine vane with ceramic coating.

I. Relationship between the ceramic coating effectiveness and the internal cooling intensity.

The heat of the combustion gas, after transmitting through the ceramic coating and turbine vane, can be carried away by the cooling air inside the vane cavity. If the internal cooling intensity is not high enough, increasing the thickness of the ceramic coating alone can not guarantee that the temperature of bond coat will not exceed 1367 K. This can be explained from the heat transfer process in a compound flat wall which consists of ceramic, bond and metal. (see Fig.1). From the thermal equilibrium equation of the heat transfer in this flat wall, the following equation can be derived.

$$\frac{T_g - T_c}{T_1 - T_c} = 1 + \left(\frac{1}{\alpha_g} + \frac{\delta_0}{\lambda_0}\right) \Big/ \left(\frac{1}{\alpha_c} + \frac{\delta_b}{\lambda_b} + \frac{\delta_m}{\lambda_m}\right) \tag{1}$$

If T_1 and T_c are fixed, then the derivative of Eq.(1) with respect to δ_c is :

$$\frac{dT_g}{d\delta_0} = \left(\frac{T_1 - T_c}{\lambda_0}\right) \Big/ \left(\frac{1}{\alpha_c} + \frac{\delta_b}{\lambda_b} + \frac{\delta_m}{\lambda_m}\right) \tag{2}$$

Whenever the thickness of the ceramic coating increases, the allowed combustion gas temperature can be increased correspondingly without damaging the bond coat. If we let the increase of allowed gas temperature after increasing 0.1 mm of ceramic coating as η, which is called the effectiveness of ceramic coating, then Eq.(2) can be rewritten as :

$$\eta \cdot 10^4 = \left(\frac{T_1 - T_c}{\lambda_0}\right) \Big/ \left(\frac{1}{\alpha_c} + \frac{\delta_b}{\lambda_b} + \frac{\delta_m}{\lambda_m}\right) \quad \text{K/0.1 毫米} \tag{2'}$$

After comparing the values of each item, we find out that the heat transfer coefficient α_c is the most important term in the denominator of Eq.(2').

The analysis above about the compound flat wall is only good for the flat section of a turbine vane. For the leading edge of the vane, the various layers have different curvature radii and then have different heat transfer areas. If Fig.1 is a compound cylinder, for instance, then the radii of each layers are : $R_2 = R_3 + \delta m$, $R_1 = R_3 + \delta_m + \delta_b$, and $R_0 = R_3 + \delta m + \delta_b + \delta_0$, Therefore, Eq.(1) will become:

$$\frac{T_g - T_c}{T_1 - T_c} = 1 + \frac{\dfrac{1}{\alpha_g(R_3 + \delta_m + \delta_b + \delta_0)} + \dfrac{\delta_0}{\lambda_0(R_3 + \delta_m + \delta_b + \delta_0/2)}}{\dfrac{1}{\alpha_c R_3} + \dfrac{\delta_m}{\lambda_m(R_3 + \delta_m/2)} + \dfrac{\delta_b}{\lambda_b(R_3 + \delta_m + \delta_b/2)}} \tag{3}$$

Take the derivative of Eq(3) with respect to δ_0, the formula of η for the leading edge of the vane can be obtained by comparing each term with the same order (lower order terms are neglected), which is

$$\eta \cdot 10^4 = \left(\frac{T_1 - T_c}{\lambda_0}\right) \Big/ \left[\frac{1}{\alpha_c}\left(1 + \frac{2\delta_m + 2\delta_b + \delta_0}{2R_3}\right) + \frac{\delta_m}{\lambda_m}\left(1 + \frac{\delta_m + 2\delta_b + \delta_0}{2R_3 + \delta_m}\right) + \frac{\delta_b}{\lambda_b}\left(1 + \frac{\delta_b + \delta_0}{2R_3 + 2\delta_m + \delta_b}\right)\right] \tag{4}$$

1131

Comparing Eq.(4) with Eq.(2'), it can be seen that the η value of the

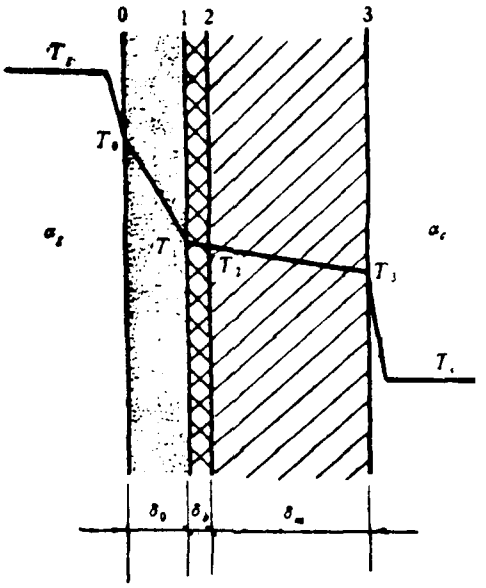

Fig.1. Schematic diagram of the heat transfer in the turbine vane with ceramic coating.

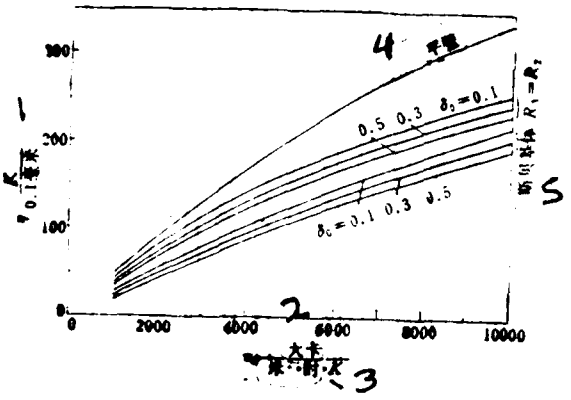

Fig.2. The coating effectiveness of the turbine vane with ceramic coating. (1: mm; 2: Kcal; 3: m^2 hr; 4: flat surface; 5: SPEY body)

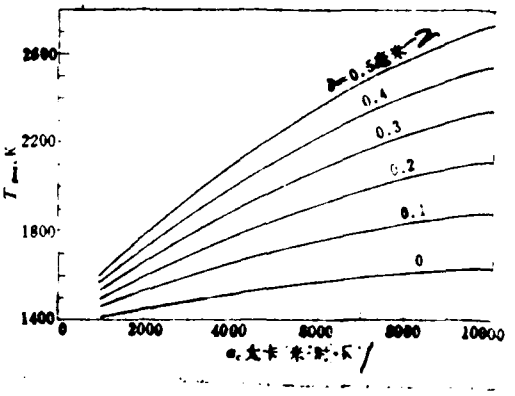

Fig.3. The maximum allowed gas temperature vs the thickness of ceramic coating and the internal cooling intensity. (1: Kcal/m^2 hr; 2: mm)

leading edge is much smaller than that of the flat section. The η value of the leading edge also decreases with increasing the thickness of the ceramic coating, δ_c. Therefore, the value of δ_c should not be too large.

It can be seen from Eq.(4) that increasing the inner radius R_3 of the vane's leading edge can alleviate the decreasing of η, where the decreasing of η is caused by the fact that each layer has a different curvature radius. If the curvature radius R_3 of the vane's leading edge is equal to R_2, then Eq.(4) will become:

$$\eta \cdot 10^4 = \left(\frac{T_1 - T_c}{\lambda_0}\right) \Big/ \left[\frac{1}{a_c}\left(1 + \frac{2\delta_b + \delta_0}{2R_3}\right) + \frac{\delta_m}{\lambda_m}\left(1 + \frac{2\delta_b + \delta_0}{2R_3}\right) + \frac{\delta_b}{\lambda_b}\left(1 + \frac{\delta_b + \delta_0}{2R_3 + \delta_b}\right)\right] \qquad (5)$$

It is obvious that the η value calculated by Eq.(5) is higher than that calculated by Eq.(4). But in order to let $R_3 = R_2$, the curvature center of the leading edge's inner cavity should be moved backward. In this way the wall thickness, δ_m, around the station point of the vane will increase and then the heat resistance of the vane will also increase. If we take the first stage guided vane of SPEY MK202 engine as an example, then the wall thickness around the station should be increased from 0.76 mm to 1.9 mm. In order to compare these two cases, the leading edge parameters of the SPEY first stage vane, i.e. R_3 = 1.1 mm, R_2 = 1.86 mm, and δ_m= 0.76 mm are substituted into Eq.(4), and the following data, $R_3 = R_2$ = 1.86 mm and δ_m= 1.9 mm are substituted into Eq.(5). The other data which are needed in these two equations are: δ_b = 0.1 mm, R_1 = 1.96 mm, R_o =(1.96+ δ_o) mm, T_1 = 1360 K, T_c = 800 K, λ_o=1.1, and λ_m=24 Kcal/m·hr·K. The results of these two calculations are shown in Fig.2. The ceramic coating effectiveness of the flat wall is also shown in Fig.2 for comparison.

It can be seen from Fig.2 that the η value increases with increasing α_c, the η value at leading edge is much less than that at the flat section, and η value increases when $R_3 = R_2$ is employed.

In Fig.3 we show the calculated maximum allowed gas temperature T_{gmax} as the function of α_c at various δ_c, where α_j=10000 Kcal/m^2·hr·K and $R_3 = R_2$. It is obvious that T_{gmax} increases with increasing α_c and δ_c.

II. Enhanced cooling for the turbine vane with ceramic coating

As was described above, the enhanced internal cooling is very important for the turbine vane with ceramic coating. In order to enhance cooling for the turbine vane, the following methods can be employed:

1. The inner cavity of the vane is divided, according to different required cooling intensity, into front, middle, and rear cooling passages. These sections have different shapes and passage areas and are connected together in series. The cooling air after passing through these three sections will come out from the chord at the tail section. 1140

2. The inner wall of the cooling passage is cast into a rib-roughened surface with 45° tilt angle such that the heat transfer is more efficient. A lot of papers had shown that the roughened surface can improve heat transfer. The semi-empiric formula of the tube with repeated-rib roughness obtained by Webb et al.[4] has been used intensively. But according to Refs. 5-7, where the heat transfer and hydropower experiments with different passage shapes were performed, the heat transfer of tilted-rib is better than that of

horizontal repeated-rib. So far, there is no suitable formula which can be applied to the case with tilted-rib roughness. In this paper we use the Webb's formula as a substitution for our calculation. The ratio of the heat transfer augmentation Nu_r calculated by this formula and the value Nu_s calculated by Dittus-Boelter's turbulence heat transfer formula for the smooth tube is shown in Fig.4.

3. Increasing the inner radius of the vane's leading edge and casting a dented duct can enhance the cooling at the front station. The heat transfer coefficient at the sharp corner area is about 20% less than that at flat section.[8] It is not a good idea to use roughened rib at the corner area because an obstruct section will be formed and this will hurt the heat transfer enhancement. Increasing the inner radius not only will improve the heat transter at the corner area, the increased wall thickness (due to the increase of inner radius) also makes the duct casting at the corner area easier. Besides, the rib roughness at the break point of the corner area can disturb the gas flow coming from the side. According to the experiment in Ref. 9, the rib roughness can enhance the heat transfer at the area without rib by 40%. If the effect of dented duct at the corner area is also considered, then the total heat transfer coefficient at the corner area can be doubled.

4. The duct with disturbing columns at the tail section of the vane can enhance the convectional heat transter at a narrow slit. It also can solidify the structure at the tail. Since the length and diameter ratio L/d of the disturbing column is very small, the wall effect can not be neglected. The conventional heat transfer formula for the horizontal disturbing circular column can not be employed

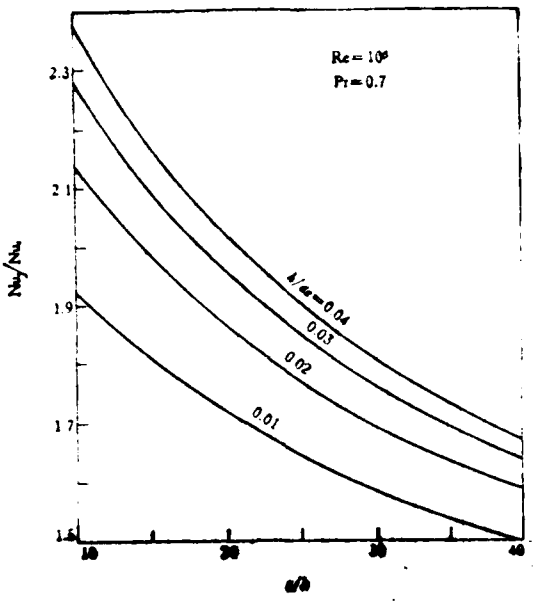

Fig. 4. The enhanced heat transfer ratio of the roughened cylindrical tube with repeated-rib.

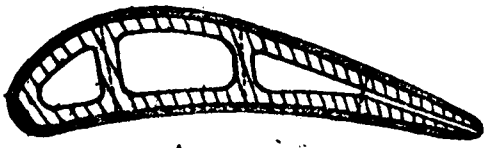

$A_1 = 15$, $A_2 = 34$, $A_3 = 15$毫米; $dc_1 = 3.87$, $dc_2 = 5.34$, $dc_3 = 3.0$毫米

Fig. 5. Turbine vane with ceramic coating and its cooling passages. (1: mm)

here; however, the empiric formula obtained by Faulkner [10] in the staggered disturbing column experiment can be used. The calculated Nu is:

$$Nu = [0.023 + 4.143Re^{-0.2946}\exp\{-3.094(d/s) - 0.89(s/L)^{0.5075}\}]Re^{0.8}Pr^{0.33} \quad (6)$$

III. Temperatures at front station of the turbine vane with ceramic coating under different conditions

In this section, the temperature at the vane's front station vs ceramic thickness is analyzed under different cooling conditions. The calculation was done on the first stage guided vane of the SPEY MK202 engine, where maximum allowed gas temperature is 1850 K. The shape and dimension of the turbine vane with ceramic coating is shown in Fig.5, and the other data are quoted from Ref. 11. Since the cooling passages are in series, the air temperature of each section is gradually increasing but the pressure is gradually decreasing. The leading edge of the vane is irradiated directly by the flame of combustion. Its thermal radiation flux is

$$q_R = A_0C[\varepsilon_f(T_f/100)^4 - (T_0/100)^4] \quad (7)$$

The energy emitted and reflected from the leading edge of the vane may come back to the vane surface again, but it is negligible. This is because the absorption coefficient A_{fo} of the combustion gas is very high. Since $A_{fo} = \varepsilon_f(T_f/T_0)^{1.5}$, where $\varepsilon_f = 1-\exp[-2.9\times10^{-4}Lp(rl)^{0.5}T_f^{1.5}]$ [12] The value of A_{fo} can be determined, by substituting the known values into the above expression, to be 0.93. So, the radiation energy, after passing through the combustion gas, will become very small when it comes back to the vane surface.

In order to allow for unforeseen circumstances, the absorption

coefficient A_o if the ceramic coating is assumed to be 1.0.

Substituting T_g = 2100 K into Eq. (7), then we have:

$$q_R = 2.48[13.2 \cdot 10^4 - (T_0/100)^4]$$

Substituting α_{gc}=8710 Kcal/m^2·hr·K, which is quoted from Ref. 11, and T_g = 1850 K into the convectional heat transfer formula, then we have

$$q_c = 8710(1850 - T_0)$$

the total thermal flux at the front station of the vane is then

$$q_0 = q_c + q_R = 8710(1850 - T_0) + 2.48[13.2 \cdot 10^4 - (T_0/100)^4] \quad (10)$$

On the other hand, the temperature difference between the ceramic surface and the cooling air, where $R_3 = R_2$, can be calculated by the following equation:

$$T_0 - T_c = q_0\left[\frac{2\delta_0 R_0}{\lambda_0(R_0 + R_1)} + \frac{\delta_m R_0}{\lambda_m R_3} + \frac{2\delta_1 R_0}{\lambda_1(R_1 + R_3)} + \frac{R_0}{\alpha R_h}\right] \quad (11)$$

The average cooling air temperature T_C can be calculated from the heat transfer formula for the front section of the vane (see next section), where s/h=10, h/de is varied, α_c is obtained from the Webb's formula [4], and the weakened coefficient at the corner area is 0.8. Substituting various values of α_c and δ_c into Eqs. (10) and (11), T_o then can be determined by iteration method. When T_o is known, T_1 also can be determined. These results are shown in Fig.6. From the calculation, we find out that, by using δ_c=0.1 m, h/de=0.01, and s/h=10, the temperature T_1 at the front station can be assured less than 1367 K. Figure 6 also indicates that T_1 and T_o can be reduced remarkably by using roughened surfaces. The variation of the roughness parameters, however, only has a small effect on the values of T_1 and T_o. Therefore, for the purpose of real application, a passage with a bigger size of roughness is better than a passage with optimal

roughness parameter. For the calculation in the next section, the roughness parameters: h_c/d_e=0.03 and s/h=2.5 are employed.

IV. Temperature distribution in the turbine vane with ceramic plating

Using the roughness parameters mentioned above, i.e., δ_c = 0.2 mm and δ_b = 0.1 mm, the temperatures at the basin and the back of the different sections (front, middle and rear sections) of the vane, as well as the maximum temperatures at the front station and at the tail can be determined. The tail's maximum temperature is at the beginning of the cooling duct which is on the back side of the vane. This is because the heat transfer coefficient is the highest at this position. Let's first calculate the temperature increment, T_c, of the air in the cooling passage. Since

/42

$$dQ = \alpha_c (T_w - T_c) dF_c = G_c c_{p_c} dT_c ,$$

ΔT_c can be obtained by integrating this expression, which is

$$\Delta T_c = (\bar{T}_w - T_{c1})(1 - e^{-m}) \tag{12}$$

where $m = (\alpha f / G c_p)_c$, T_{c1} is the cooling air temperature at the passage inlet, and $\bar{T}_w$ is the average wall temperature between the vane basin and the vane back of that section.

Since the gas temperature, gas pressure, passage cross section, and the surface temperature of the vane are variable, the caculation of thermal radiation flux q_R is very difficult. Since the maximum gas temperature is only 1850 K, q_R is estimated to be about 3% of the value of q_c. Since the effect of radiation heat transfer must be taken into consideration, $q_o = 1.03\, q_c$ is used here just for simplicity. The temperature of the inner wall in the cooling passage can thus be determined by the following equation:

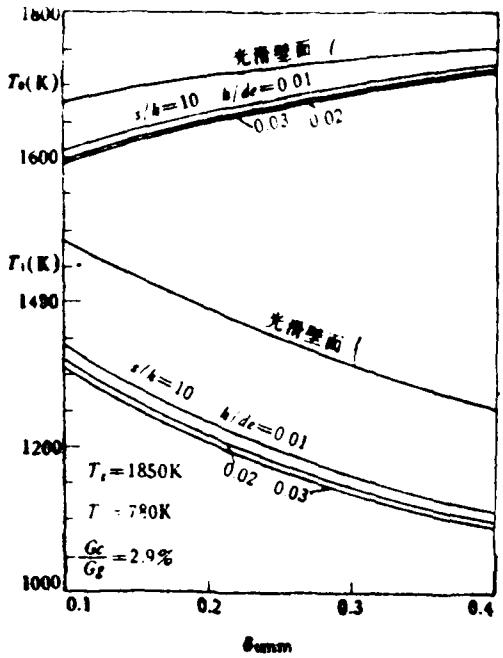

Fig. 6 The temperatures of ceramic coating and bond coat at the front station of the turbine vane. (1: smooth surface)

项 目 1		驻点温度 2	前部温度 3	中部温度 4	后部温度 5	尾部温度 6
7 叶背	T_0	1661	1602	1589	1573	1591
	T_1	1234	1229	1263	1249	130
8 叶盆	T_0		1519	1463	1468	
	T_1		1184	1182	1169	
9 冷气	进口温度 K 10		780	830	867	900
	进口压力 atm 11		19.7	15.6	15.2	14.0

Table (1: item; 2: temperature at station; 3: temperature at front section; 4: temperature at middle section; 5: temperature at rear section; 6: temperature at tail section; 7: vane back; 8: vane basin; 9: cooling air; 10: inlet temperature; 11: inlet pressure)

$$\frac{T_\infty - \bar{T}_c}{T_g - \bar{T}_c} = \frac{1.03}{\alpha_c U_3} \Big/ \left[\frac{1}{\alpha_g U_0} + \frac{2.06\delta_0}{\lambda_0(U_0 + U_1)} + \frac{2.06\delta_b}{\lambda_b(U_1 + U_2)} + \frac{2.06\delta_m}{\lambda_m(U_2 + U_3)} + \frac{1.03}{\alpha_c U_3}\right].$$

The values of $\bar{T}_\omega$, ΔT_c, and $\bar{T}_c$ can be calculated from this equation and Eq. (12) by iteration method. The temperature at bond coat, T_1, can be calculated by

$$\frac{T_g - T_1}{T_g - \bar{T}_c} = \left[\frac{1}{\alpha_g U_0} + \frac{2.06\delta_0}{\lambda_0(U_0 + U_1)}\right] \Big/ \left[\frac{1}{\alpha_g U_0} + \frac{2.06\delta_0}{\lambda_0(U_0 + U_1)} + \frac{2.06\delta_b}{\lambda_b(U_1 + U_2)} + \frac{2.06\delta_m}{\lambda_m(U_2 + U_3)} + \frac{1.03}{\alpha_c U_3}\right].$$

A 0.6 mm slit is made on the tail of the vane such that cooling can be achieved by convection. According to calculation, smooth passage is good enough for heat transfer here; the disturbing column to enhance heat transfer is thus not necessary. For the turbine vane with ceramic coating, which has the maximum allowed gas temperature 1850 K and cooling air flow rate ratio 2.9%, the calculated surface temperature T_0 and bond temperature T_1 are listed in the table below. The maximum restriction value for T_1 is at the beginning of the cooling duct of the tail. This value is 60 K less than the maximum allowed temperature of 1367 K.

IV. Conclusion

1. The ceramic coating can reduce the vane temperature effectively. In order to prevent bond temperature higher than 1367 K, the internal cooling of the vane must be enhanced. The ceramic coating's effectiveness increases rapidly with the increase of the internal cooling intensity.

2. The ceramic coating effectiveness is maximum at the flat

section of the vane. At the leading edge, due to the curved coating, the external heat transfer area becomes bigger. Besides of this, the η value decreases. It will decrease even more with increasing η value. This shortcoming can be alleviated by increasing the inner curvature diameter of the leading edge.

3. The internal cooling can be enhanced by using a roughened surface and by series connection for all cooling passages. The roughness parameter has little effect on the bond temperature. So, it is better to use the roughness element with higher values of h/de and s/h, which is easier to be made technically, such that the maximun allowed gas temperature can be increased to more than 2000 K.

4. The calculation for the thermal performance of the SPEY MK202 turbine vane with ceramic coating and enhanced cooling shows that, by employing appropriate cooling structure and 0.2 mm of ceramic coating, the maximum allowed gas temperature of 1850 K can be reached by using only 2.9% of cooling air. This implies that the average temperature in front of the turbine is 1600 K.

References:

[1] Halback C. R. et al.: AIAA Paper 74—154, (1974).

[2] Liebert C. H. Stepka F. S.: Ceramic Thermal Barrier Coatings for Cooled Turbines, J. Aircraft, 14, 5, (1977), 487.

[3] Singhal S. C., Bratton R. J.: Stability of a $ZrO_2(Y_2O_3)$ Thermal Barrier Coating in Turbine Fuel with Contaminants, J. Eng. Power, 102, (1980), 770.

[4] Webb R. L. et al.: Heat Transfer and Friction in Tubes with Repeated-Rib Roughness, Int. J. Heat Mass Transfer, 14, 4, (1971), 601.

[5] Han J. C. et al.: An Investigation of Heat Transfer and Friction for Rib-Roughened Surfaces, Int. J. Heat Mass Transfer, 21, 8, (1978), 1143.

[6] Pirie M. A. M.: Heat Transfer and Pressure Drop Tests on Multi-Start Ribbed Surface Covering the Rib Angle Range 0° to 60°, RD/B/N-2760, (1974).

[7] Withers J. G.: Tube-Side Heat Transfer and Pressure Drop for Tubes Having Helical Internal Ridging with Turbulent/Transitional Flow of Single-Phase Fluid, Part 2. Multiple-Helix Ridging, Heat Transfer Eng. 2, 2, (1980), 43.

[8] Lowdermilk W. M. et al.: Measurement of Heat Transfer and Friction Coefficients for Flow of Air in Noncircular Ducts at High Surface Temperatures, NACA RM E53J07, (1953).

[9] Burggraf F.: Experimental Heat Transfer and Pressure Drop with Two-Dimensional Discrete Turbulence Promoters Applied to Two-Opposite Walls of a Square Tube, Augmentation of Convective Heat and Mass Transfer, ASME (1970), New York.

[10] Faulkner F. E.: Analytical Investigation of Chord Size and Cooling Methods on Turbine Blade Cooling Requirements, NASA CR120882, (1971).

[11] "SPEY MK202 HPI NGV Cooling Design Report" TBD12001, (1976), R. R. Corp.

[12] Lefebvre A. H., Herbert M. V.: Heat Transfer Processes in Gas-Turbine Combustion Chambers, Proc. Inst. Mech Engrs, 174, 12, (1960), 463.

END

DTIC

8-86